

NFI-C Regulates Osteoblast Differentiation via Control of Osterix Expression

DONG-SEOL LEE,^{a,b} HAN-WOOL CHOUNG,^a HEUNG-JOONG KIM,^b RICHARD M. GRONOSTAJSKI,^c YOUNG-IL YANG,^d HYUN-MO RYOO,^e ZANG HEE LEE,^e HONG-HEE KIM,^e EUI-SIC CHO,^f JOO-CHEOL PARK^a

Key Words. Bone marrow stromal cells • Osteoblast • Adipogenesis • Osteoporosis • Differentiation • Proliferation

^aDepartment of Oral Histology-Developmental Biology and ^eSchool of Dentistry and Dental Research Institute, Seoul National University, Chongro-gu, Seoul, Korea; ^bDepartment of Anatomy and Orofacial Development, School of Dentistry, Chosun University, Dong-gu, Gwangju, Korea; ^cDepartment of Biochemistry, Developmental Genomics Group, State University of New York at Buffalo, Buffalo, New York, USA; ^dPaik Institute Clinical Research, Inje University, Busan-Jin-gu, Busan, Korea; ^fLaboratory for Craniofacial Biology, Institute of Oral Bioscience, Chonbuk National University, Deokjin-gu, Jeonju, Korea

Correspondence: Joo-Cheol Park, D.D.S., Ph.D., Department of Oral Histology-Developmental Biology, School of Dentistry, Seoul National University, 101 Daehagro, Chongro-gu, Seoul 151-749, Korea. Telephone: 82-2-740-8668; Fax: 82-2-763-3613; e-mail: jcpark@snu.ac.kr

Received December 24, 2013; accepted for publication March 30, 2014; first published online in *STEM CELLS EXPRESS* May 6, 2014.

© AlphaMed Press
1066-5099/2014/\$30.00/0

<http://dx.doi.org/10.1002/stem.1733>

ABSTRACT

In bone marrow, bone marrow stromal cells (BMSCs) have the capacity to differentiate into osteoblasts and adipocytes. Age-related osteoporosis is associated with a reciprocal decrease of osteogenesis and an increase of adipogenesis in bone marrow. In this study, we demonstrate that disruption of nuclear factor I-C (NFI-C) impairs osteoblast differentiation and bone formation, and increases bone marrow adipocytes. Interestingly, NFI-C controls postnatal bone formation but does not influence prenatal bone development. We also found decreased NFI-C expression in osteogenic cells from human osteoporotic patients. Notably, transplantation of *Nfic*-overexpressing BMSCs stimulates osteoblast differentiation and new bone formation, but inhibits adipocyte differentiation by suppressing peroxisome proliferator-activated receptor gamma expression in *Nfic*^{-/-} mice showing an age-related osteoporosis-like phenotype. Finally, NFI-C directly regulates Osterix expression but acts downstream of the bone morphogenetic protein-2-Runx2 pathway. These results suggest that NFI-C acts as a transcriptional switch in cell fate determination between osteoblast and adipocyte differentiation in BMSCs. Therefore, regulation of NFI-C expression in BMSCs could be a novel therapeutic approach for treating age-related osteoporosis. *STEM CELLS* 2014;32:2467–2479

INTRODUCTION

Bone marrow stromal cells (BMSCs) have the capacity to differentiate into osteoblasts and adipocytes [1, 2]. Osteogenesis is regulated by several growth and transcription factors, such as transforming growth factor β , bone morphogenetic proteins (BMPs), Wnt, Hedgehog, Runx2, Osterix (Osx), and β -catenin, whereas adipogenesis is controlled by peroxisome proliferator-activated receptor gamma (PPAR γ) [3–6]. With aging, BMSCs become inclined to undergo differentiation into adipocytes, resulting in an increased number of adipocytes and a decreased number of osteoblasts in bone marrow [7]. However, the mechanism underlying this differentiation switch remains unknown.

The nuclear factor I (NFI) family members of transcription factors are expressed from four highly conserved genes in mammals (named *Nfia*, *Nfib*, *Nfic*, and *Nfix*) [8, 9]. All four NFI genes are expressed in human osteoblasts and osteoblast-like cell lines. In particular, *Nfic* mRNA is highly expressed in normal osteoblasts compared with other NFI family members [10]. In addition, *Nfic*^{-/-} mice showed defects in alveolar bone formation in molar tooth sockets [11].

However, the exact role of NFI-C in osteoblast differentiation and bone formation remains unclear.

Oxidative stress caused by increased intracellular reactive oxygen species (ROS) also affects age-related osteoporosis and osteoblast differentiation [7]. ROS changes target gene expression by controlling transcription factor activities, such as Wnt/ β -catenin, NF κ B, JNKs, and MAPKs [12]. Oxidative stress also inhibits *Nfic* transcriptional activity [13].

In this study, we found an age-related decrease in *Nfic* expression in BMSCs. *Nfic*^{-/-} mice show an age-related osteoporosis-like phenotype with decreased osteoblast differentiation and increased adipocyte differentiation. In contrast, *Nfic* overexpression reduced adipocyte differentiation through suppression of PPAR γ , but increased osteoblast differentiation in *Nfic*^{-/-} BMSCs. These findings suggest that NFI-C is an important factor regulating the balance between osteoblast and adipocyte differentiation in BMSCs.

MATERIALS AND METHODS

Animals

All experiments involving mice were performed according to the Dental Research Institute

guidelines and the Institutional Animal Care and Use Committees of Seoul National University (SNU-111013-2). *Nfic*^{-/-} mice were generated by removal of the second exon from *Nfic* gene were kindly provided by Dr. Richard M. Gronostajski [11], and homozygous *Nfic*^{-/-} mice were obtained by crossing male and female heterozygous *Nfic*^{+/-} mice. As *Nfic*^{-/-} mice have brittle teeth, a ground standard rodent chow was provided to all animals three times a week beginning 3 days prior to weaning and continued it for up to 6 weeks. *Runx2*^{-/-} mice were kindly provided by Dr. Toshihisa Komori (Nagasaki University Graduate School of Biomedical Sciences, Nagasaki, Japan).

Micro-CT and Histomorphometric Analyses

The mandible, maxilla, and femur from 6-week-old wild-type (WT) and *Nfic*^{-/-} mice were removed, fixed in 4% paraformaldehyde at 4°C overnight, and analyzed by micro-CT with a SkyScan scanner and the associated software (Skyscan 1172, Kontich, Belgium). Isotopic resolution of the instrument was 10 µm. The 6-week-old male mice were injected with 15 mg/kg of calcein (Sigma-Aldrich, St. Louis, MO) 7 and 2 days before sacrifice. Histomorphometric analyses were performed using the OsteoMeasure histomorphometry system (OsteoMetrics, Decatur, GA).

Histology and IHC

The femurs were fixed overnight in 4% paraformaldehyde at 4°C. Undecalcified and decalcified femurs were sectioned and subjected to H&E, von Kossa, tartrate-resistant acid phosphatase (TRAP), and IHC staining [14].

Human control and osteoporotic patient bone sections were kindly provided from Dr. Y.-I. Yang (Paik Institute Clinical Research, Inje University, Korea). Bone sections were obtained from three osteoporotic patients (67–73-year-old females) with age and sex matched control group (68–75-year-old females, *n* = 3), who did not have any endocrine and metabolic diseases such as hyperparathyroidism and vitamin D deficiency. Sections were subjected to H&E and IHC staining. The study was approved by the hospital's Institutional Review Board (IRB NO: S-D20110001). The experiments were performed with the understanding and written consent of each participating subject according to the Declaration of Helsinki.

Cell Culture and Transfection

BMSCs of the tibia and femur of 6-week-old WT and *Nfic*^{-/-} mice were flushed with α -MEM (Gibco BRL, Carlsbad, CA). After removing red blood cells, cells were seeded on 100 mm culture dishes (Nunc, Rochester, NY), and cultured in α -MEM supplemented with 100 IU/ml penicillin, 100 µg/ml streptomycin (Gibco BRL), and 10% fetal bovine serum (FBS, Gibco BRL). Primary calvarial osteoblasts were isolated from the calvarial bones of WT and *Nfic*^{-/-} mice at P3 and P5. Briefly, the calvarial bones were dissected and washed in phosphate buffered saline (PBS), and cut into small pieces. Bones were digested in 1% Collagenase Type I (Gibco BRL) and 1.6% Dispase II (Gibco BRL) in α -MEM for 1 hour in a 5% CO₂ incubator. To induce osteogenic differentiation, 80%–90% confluent cells were cultured in α -MEM supplemented with 5% FBS, ascorbic acid (50 µg/ml), and β -glycerophosphate (10 mM) for up to 2 weeks. To induce adipogenic differentiation, 80%–90% confluent cells were cultured in DMEM supplemented with 10% FBS, insulin (10 µg/ml), dexamethasone (1 µM), and 3-

isobutyl-1-methylxanthine (0.5 mM) for up to 7 days. Adipocytes were identified using an oil red O staining. For the quantification, oil red O dye was extracted using isopropanol for 10 minutes at room temperature, and absorbance was measured at 510 nm.

MC3T3-E1 cells were cultured in α -MEM supplemented with 10% FBS and antibiotics. C2C12 cells (ATCC) were cultured in DMEM supplemented with 100 IU/ml penicillin, 100 µg/ml streptomycin, and 10% FBS. The indicated expression plasmid (2 µg) was transiently transfected into MC3T3-E1 and C2C12 cells using the Lipofectamine Plus reagent (Invitrogen, Carlsbad, CA) according to the manufacturer's instructions. Human BMSCs (hBMSCs) were purchased from Cambrex (East Rutherford, NJ) and cultured in low DMEM supplemented with 100 IU/ml penicillin, 100 µg/ml streptomycin, and 10% FBS.

In Vitro Osteoclastogenesis

Bone marrow cells were cultured for 1 day with 30 ng/ml Macrophage-colony stimulating factor (M-CSF) in α -MEM containing 10% FBS, and used as bone marrow-derived macrophages (BMMs). The BMMs (5×10^4 cells/well) were cultured for 3 days with M-CSF (60 ng/ml) and RANKL (100 ng/ml). In the coculture system, BMMs (5×10^5 cells/well) and calvarial osteoblasts (2.5×10^4 cells/well) were plated in each well of 48-well plates and cultured for 6 days in 400 µl α -MEM supplemented with 10% FBS, 10^{-8} M 1,25-dihydroxyvitamin D₃, and 10^{-6} M prostaglandin E₂. Osteoclasts were identified using a TRAP staining kit (Sigma-Aldrich) according to the manufacturer's instructions.

Bone Marrow Cavity Transplantation of BMSCs

Six-week-old male *Nfic*^{-/-} mice were used as recipients. BMSCs were obtained from the tibia and femur of 6-week-old *Nfic*^{-/-} mice. *Nfic*^{-/-} BMSCs were labeled with green fluorescent protein (GFP) using a retrovirus, and then cultured for 24 hours with *Nfic* or *Osx* retrovirus. We injected *Nfic*- or *Osx*-overexpressing BMSCs, or corresponding mock-infected (GFP-labeled) BMSCs (1×10^6 cells/femur in 10 µl of α -MEM) into the bone marrow cavity of the left femur. Mice were sacrificed 4 weeks after transplantation, and femurs were resected and analyzed using micro-CT.

Reverse Transcription-Polymerase Chain Reaction and Real-Time Polymerase Chain Reaction Analyses

Total RNA (2 µg) was reverse transcribed using 0.5 µg of Oligo(dT) and 1 µl (50 IU) of Superscript III enzyme (Invitrogen) in a 20 µl reaction mixture at 50°C for 1 hour. The resulting mixture was amplified by polymerase chain reaction (PCR). For real-time PCR, specific primers for *Nfic*, *Bsp*, *osteocalcin* (*Oc*), *Alp*, *Runx2*, *Osx*, *Opg*, *Rankl*, *Dlx5*, *Msx2*, *Ppar γ* , and *Hprt* were synthesized as listed in Supporting Information Table S1. Real-time PCR was performed on an ABI PRISM 7500 sequence detection system using the SYBR GREEN PCR Master Mix (Applied Biosystems, Foster City, CA) according to the manufacturer's instructions. The PCR conditions were 94°C for 1 minute, followed by 95°C for 15 seconds, and 60°C for 34 seconds for 40 cycles. All reactions were run in triplicate and were normalized to the housekeeping gene, *Hprt*. Relative differences in PCR results were calculated using the comparative cycle threshold (C_T) method.

Western Blot Analyses

Western blot analyses were performed as previously described [14]. Briefly, proteins (30 μ g) were separated by 10% sodium dodecyl sulfate polyacrylamide gel electrophoresis, transferred onto a nitrocellulose membrane (Schleicher & Schuell BioScience, Dassel, Germany), and labeled with specific antibodies. Labeled protein bands were detected using an enhanced chemiluminescence system (GE Healthcare, Buckinghamshire, U.K.).

ChIP Assays

ChIP assays were performed as previously described [15]. MC3T3-E1 cells were treated with BMP-2 (300 ng/ml) for 48 hours. The samples were sonicated, followed by chromatin immunoprecipitation with rabbit anti-mouse Nfic (30 μ l) and rabbit anti-mouse Runx2 (10 μ l, Santa Cruz) antibodies. The final DNA pellets were recovered and analyzed by PCR using specific primers. PCR primers were synthesized as listed in Supporting Information Table S2. The following PCR conditions were used: 94°C for 30 seconds; 60°C for 30 seconds; and 72°C for 30 seconds for a total of 35 cycles. The PCR products were electrophoresed in a 2% agarose gel, stained with ethidium bromide, and visualized under ultraviolet light.

Gene-Expression Profiling

Gene profiling of the two groups of hBMSCs (hBMSCs-Old and hBMSCs-OP) was described previously [16]. Publicly available gene expression datasets were downloaded from gene expression omnibus (GEO) (accession number GSE35959), and *NFI-C* mRNA expression (Probeset ID 213298_at) was analyzed between hBMSCs of five osteoporotic patients (hBMSCs-OP; 79–94 years old) and hBMSCs of the age-matched control group (hBMSCs-old donors; 79–89 years old, $n = 4$).

Statistical Analyses

All quantitative data are presented as the mean \pm SD. Statistical differences were analyzed using Student's *t* tests (*, $p < .05$).

RESULTS

Nfic Disruption Impairs Bone Formation During Postnatal Osteogenesis

First, to examine the pattern of *Nfic* gene expression with advancing age, we analyzed *Nfic* mRNA expression in BMSCs derived from embryonic day 18.5 (E18.5) to 60-week-old mice. After birth, *Nfic* expression significantly increased from postnatal day 16 (P16) to 6 weeks, and subsequently decreased by 60 weeks (Fig. 1A). During in vitro osteoblast differentiation, *Nfic* was expressed from day 0 of the culture, increased from days 4 to 10 (early osteoblast differentiation), and decreased by days 10–21 (late osteoblast differentiation and mineralization). Runx2 expression increased from days 4 to 7, and then declined gradually from days 10 to 21, corresponding to late osteoblast differentiation and mineralization, at which period showed the peak expression of *Osx* during culture (Fig. 1B).

Nfic^{-/-} mice have normal life spans but showed growth retardation due to impaired ability to feed on hard, normal rodent chow from delayed tooth root development [11].

Therefore, to mitigate feeding impairment in *Nfic*^{-/-} mice, we added a soft dough dietary supplement 3 days prior to weaning and continued it for up to 6 weeks, and measured the body weight of WT and *Nfic*^{-/-} mice. The total weight difference between WT and *Nfic*^{-/-} mice at 16 days and 6 weeks was not significant (Supporting Information Fig. S1A). After rescuing *Nfic*^{-/-} mice from the impaired feeding-dependent growth retardation using the soft dough diet, we evaluated the effect of *Nfic* disruption on the mandible using microcomputed tomography (micro-CT) at 6 weeks of age. In addition to the previous characterized defects in tooth roots, the cortical bone volume and bone thickness were markedly reduced in the mandible of *Nfic*^{-/-} mice compared to WT (Fig. 1C). These results suggest that *Nfic* disruption markedly reduces bone volume, which is not a starvation effect on bone density.

To investigate the role of *Nfic* in bone, we examined the bone microarchitecture in *Nfic*^{-/-} femurs at 6 weeks. Micro-CT images of femoral bone showed decreased trabecular bone volume and cortical bone thickness in *Nfic*^{-/-} mice compared to WT (Fig. 1D, 1E). We analyzed both males and females by histology and found no sex differences regarding reduced trabecular bone density and increased trabecular bone separation. To reduce variation, we used only male littermates for all the experiments. In micro-CT analyses, *Nfic*^{-/-} mice exhibited significant decreases in bone mineral density (32%), trabecular bone volume (BV/TV, 34%), trabecular bone number (Tb.N, 41%), cortical bone volume (Ct.BV/TV, 24%), and cortical bone thickness (Ct.Th, 20%), but a significant increase in trabecular separation (Tb.SP, 34%; Fig. 1F). We also investigated the effects of *Nfic* disruption on bone sampled during the lactation period, at postnatal day 16 (P16) where impaired feeding did not occur. As expected, mice at P16 and 6 weeks showed very similar bone characteristics (Supporting Information Fig. S1B, S1C), suggesting that *Nfic* disruption impairs bone formation during postnatal osteogenesis. However, *Nfic*-deficiency did not affect prenatal bone and tooth development (Supporting Information Fig. S2A–S2D). Overall, these results are consistent with the notion that *Nfic* controls postnatal bone formation and tooth root development but does not influence prenatal bone development.

To determine whether the decreased bone mass of *Nfic*^{-/-} mice was caused by impaired osteoblast activity, we evaluated osteoblast function using bone histomorphometric analyses in 6-week-old femurs. Trabecular and cortical bone volume were markedly decreased in *Nfic*^{-/-} mice compared to WT based on H&E and von Kossa staining (Fig. 1G). Osteoblast number per tissue area (N.Ob/T.Ar), osteoblast number per bone parameter (N.Ob/B.Pm), osteoblast surface per bone surface (Ob.S/BS), mineralizing surface per bone surface (MS/BS), and bone formation rate per bone surface were significantly decreased in *Nfic*^{-/-} mice compared to WT (Fig. 1H). *Nfic*^{-/-} mice at P16 had similarly reduced parameters of osteoblast activity as the 6-week-old mice (Supporting Information Fig. S1D, S1E). To determine whether the reduced osteoblast number in *Nfic*^{-/-} mice resulted from the decreased proliferation of bone forming osteoblasts, we evaluated the cell proliferation rate by IHC using PCNA antibody as well as MTT assays. We also investigated the expression of cell cycle arrest protein, p21, by Western blot. In the femur, proliferating cell nuclear antigen (PCNA)-positive cells were dramatically decreased in osteogenic cells from

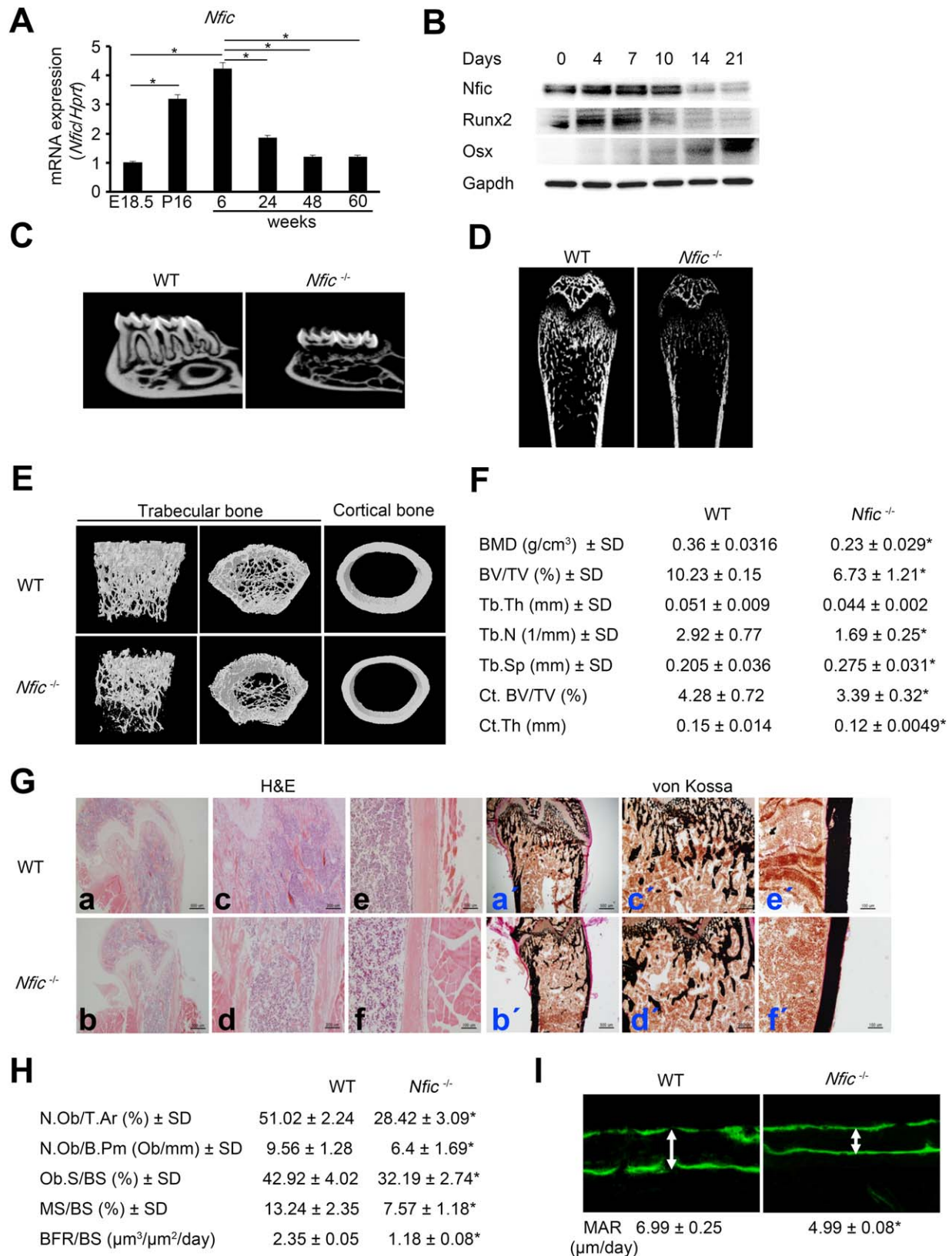


Figure 1. *Nfic* disruption impairs bone formation during postnatal osteogenesis. **(A):** *Nfic* expression was evaluated using real-time PCR analyses in bone marrow stromal cells derived from aged mice. $n = 3$, $*$, $p < .05$. **(B):** MC3T3-E1 cells were cultured in differentiation media for up to 3 weeks. *Nfic*, *Runx2*, and *Osx* were evaluated using Western blot analyses. **(C):** Representative micro-CT image of the mandible and **(D)** the distal femur. **(E):** 3D micro-CT images of trabecular bone and cortical bone in the distal femur. **(F):** Micro-CT quantification of the distal femur in WT and *Nfic*^{-/-} mice aged 6 weeks. $n = 5$, $*$, $p < .05$. **(G):** H&E staining (a-f) and von Kossa staining (a'-f') from distal femurs in WT and *Nfic*^{-/-} mice aged 6 weeks. c-f and c'-f' are higher magnifications of a-b and a'-b', respectively. c-d and c'-d', trabecular bone. e-f and e'-f', cortical bone. Scale bars, a-b and a'-b' = 500 μm; c-d and c'-d' = 200 μm; e-f and e'-f' = 100 μm. **(H):** Histomorphometric analyses of distal femoral metaphysis in WT and *Nfic*^{-/-} mice aged 6 weeks. $n = 5$, $*$, $p < .05$. **(I):** Representative calcein double labeling sections in femurs from WT and *Nfic*^{-/-} mice aged 6 weeks. The white arrow represents the MAR. $n = 5$, $*$, $p < .05$. Data are presented as the mean ± SD. Abbreviations: BFR/BS, bone formation rate per bone surface; BMD, bone mineral density; BV/TV, trabecular bone volume; Ct.BV/TV, cortical bone volume; Ct.Th, cortical bone thickness; MAR, mineral apposition rates; MS/BS, mineralizing surface per bone surface; N.Ob/B.Pm, osteoblast number per bone parameter; N.Ob/T.Ar, osteoblast number per tissue area; Ob.S/BS, osteoblast surface per bone surface; Tb.Th, trabecular bone thickness; Tb.N, trabecular bone number; Tb.Sp, trabecular separation; WT, wild type.

Nfic^{-/-} mice compared to WT (Supporting Information Fig. S3A). In vitro 3-(4,5-dimethylthiazol-2-yl)-2,5-diphenyltetrazolium bromide (MTT) assays showed decreased proliferation rates, with a 35% decrease in *Nfic*^{-/-} BMSCs (Supporting Information Fig. S3B). Furthermore, *Nfic*^{-/-} BMSCs exhibited an increase in p21 but a decrease in cyclin D1 (Supporting Information Fig. S3C). The distance of double calcein labeling was reduced in *Nfic*^{-/-} mice compared to WT, indicating that the mineral apposition rate was significantly reduced (by ~30%) in *Nfic*^{-/-} mice (Fig. 1I). These experiments suggest that the loss of *Nfic* in mice results in reduced osteoblast number and impaired osteoblast function in bone.

***Nfic*-Deficiency Increases Bone Marrow Fat Similar to Osteoporotic Patients**

To determine whether the decreased bone mass in *Nfic*^{-/-} mice resulted from an increased number of bone marrow adipocytes, we evaluated bone marrow adipocytes in the femurs from *Nfic*^{-/-} mice using H&E staining. There was greater accumulation of adipocytes in the bone marrow space of *Nfic*^{-/-} mice that increased in an age-dependent manner (Fig. 2A). To investigate the effect of *Nfic* disruption on adipocyte differentiation of BMSCs, we evaluated adipocyte differentiation using oil red O staining after culturing WT and *Nfic*^{-/-} BMSCs. Oil red O-positive cells were dramatically increased in *Nfic*^{-/-} BMSCs compared to WT BMSCs in control and adipogenic induction media (Fig. 2B, upper left panel). The amount of oil red O dye was significantly increased in *Nfic*^{-/-} BMSCs (Fig. 2B, upper right panel). Expression of the adipocyte differentiation marker, *Pparγ*, was significantly increased in *Nfic*^{-/-} BMSCs (Fig. 2B, lower panel). However, there were no differences between WT and *Nfic*^{-/-} BMSCs with respect to oil red O positivity or *Pparγ* expression at E18.5 (Supporting Information Fig. S2E).

Marrow adipocytes were also increased in the bone sections of osteoporotic patients as observed in *Nfic*^{-/-} mice (Fig. 2C). Thus, we evaluated NFI-C and CD68 expressions using IHC analyses of the bone from normal and osteoporotic patients. NFI-C was strongly detected in osteoblasts of normal bone, but was dramatically decreased in osteoporotic bone. The number of CD68-positive osteoclasts was markedly decreased in osteoporotic patient bone compared to normal (Fig. 2D). Next, we analyzed *NFI-C* mRNA expression using the microarray dataset that was used to compare the gene expression pattern between osteoporosis hBMSCs (hBMSCs-OP) and control hBMSCs (hBMSCs-old) in GEO (accession no. GSE35959). In this dataset, *NFI-C* gene expression was significantly decreased in hBMSCs-OP compared to hBMSCs-Old (Fig. 2E). ROS also affects age-related osteoporosis by controlling target gene expression [7]. Therefore, to investigate the effect of ROS on *NFI-C* expression, we evaluated *NFI-C* expression using real-time PCR and Western blotting after H₂O₂ treatment of hBMSCs. *NFI-C* mRNA and protein levels were significantly decreased in H₂O₂-treated hBMSCs compared to control cells (Fig. 2F). These results suggest that *NFI-C* is a potential candidate gene for age-related osteoporosis.

***Nfic* Accelerates Osteoblast Differentiation and Suppresses Adipocyte Differentiation**

To investigate the effect of *Nfic* overexpression on osteoblast and adipocyte differentiation of *Nfic*^{-/-} BMSCs, we incubated cells in osteogenic differentiation media for 14 days or adipo-

genic differentiation media for 7 days after transient transfection of *Nfic* expression plasmid into *Nfic*^{-/-} BMSCs. Osteoblast and adipocyte differentiation were evaluated using real-time PCR, alkaline phosphatase (ALP) staining, alizarin red S mineralization, and oil red O staining. *Nfic* overexpression increased ALP activity and mineralized nodules in *Nfic*^{-/-} BMSCs (Fig. 3A). *Alp* mRNA expression also increased with *Nfic* overexpression in *Nfic*^{-/-} BMSCs (Fig. 3B). However, *Nfic* overexpression decreased the number of oil red O-positive adipocytes in *Nfic*^{-/-} BMSCs (Fig. 3C). In addition, *Pparγ* expression was also significantly decreased by *Nfic* overexpression in *Nfic*^{-/-} BMSCs (Fig. 3D). Moreover, *Nfic*-overexpressing cells had 20-fold decreased *Pparγ* promoter activity approximately compared to control cells (Fig. 3E). These results suggest that *Nfic* promotes osteoblast differentiation and inhibits adipocyte differentiation by suppressing *Pparγ* expression in BMSCs.

To determine whether *Nfic* expression in BMSCs could rescue the osteoporosis-like phenotype of *Nfic*^{-/-} mice, we overexpressed *Nfic* in *Nfic*^{-/-} BMSCs via retroviral infection and transplanted these cells into the femur cavities of *Nfic*^{-/-} mice. Femur micro-CT images show that *Nfic*^{-/-} mice transplanted with *Nfic*-overexpressing BMSCs have increased trabecular bone volume compared to *Nfic*^{-/-} mice transplanted with mock-infected BMSCs (Fig. 3F, left panel). In histomorphometric analyses, *Nfic*^{-/-} mice transplanted with *Nfic*-overexpressing BMSCs exhibited significant increases in trabecular bone volume (BV/TV) and trabecular bone number (Tb.N), but significant decreases in Tb.SP (Fig. 3F, right panel). Four weeks after transplantation, the transplanted BMSCs were analyzed by IHC using the *Nfic* and GFP antibodies. In *Nfic*^{-/-} mice transplanted with *Nfic*-overexpressing BMSCs, *Nfic*- and GFP-positive cells were observed along the trabecular bone surface, indicating osteoblast differentiation of transplanted BMSCs (Fig. 3G). However, in *Nfic*^{-/-} mice transplanted with mock-infected BMSCs, only GFP-positive BMSCs were found in bone marrow without *Nfic* expression (Fig. 3G). In histological analyses, transplantation of *Nfic*-overexpressing BMSCs showed an increase in trabecular bone mass (Fig. 3G) but a decrease in bone marrow adiposity compared to *Nfic*^{-/-} mice (Fig. 3H). These results suggest that *NFI-C* may be a new target for osteoporosis treatment because *Nfic*-overexpression rescued the osteoporosis-like phenotype of *Nfic*^{-/-} mice.

***Nfic* Disruption Impairs Osteoblast Differentiation, Which Reduces Osteoclast Activity**

To investigate the effect of *Nfic* disruption on osteoblast differentiation of BMSCs, we evaluated the expression of osteoblast differentiation markers using real-time PCR, ALP staining, and alizarin red S mineralization after culturing BMSCs from WT and *Nfic*^{-/-} mice. ALP activity and quantity of mineralized nodules from alizarin red S staining in *Nfic*^{-/-} BMSCs decreased approximately twofold compared to WT cells (Fig. 4A, 4B). Expression of the osteoblast differentiation marker *Runx2* was unaffected by *Nfic* disruption. However, *Osx*, *Alp*, *osteocalcin* (*Oc*), and *bone sialoprotein* (*Bsp*) expressions were significantly decreased in *Nfic*^{-/-} BMSCs (Fig. 4C). These findings suggest that *Nfic* disruption impairs osteoblast differentiation of BMSCs.

To determine whether the decreased trabecular bone volume was caused by increased osteoclast activity in *Nfic*^{-/-}

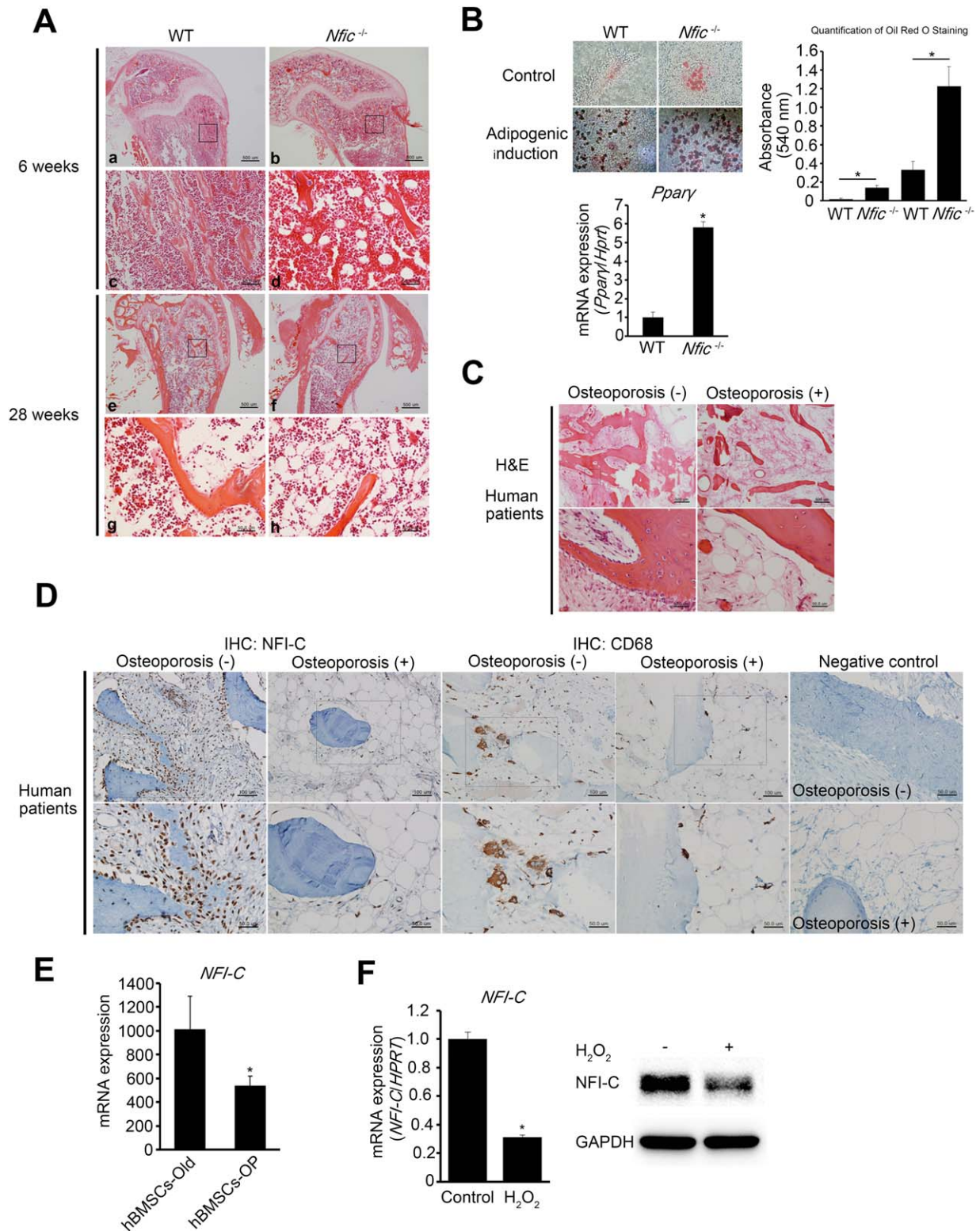


Figure 2. *Nfic*-deficiency increases bone marrow fat as seen in osteoporotic patients. **(A):** H&E staining of distal femurs from WT and *Nfic*^{-/-} mice aged 6 and 28 weeks. c-d and g-h are higher magnifications of boxed a-b and e-f, respectively. a-d, 6 weeks. e-h, 28 weeks. Scale bars = a-b and e-f = 500 μ m; c-d and g-h = 50 μ m. **(B):** Representative oil red O staining images (upper left panel) and quantification of oil red O staining (upper right panel). WT and *Nfic*^{-/-} BMSCs were cultured in adipogenic induction media for 7 days. *PPAR* γ expression was analyzed using real-time PCR in WT and *Nfic*^{-/-} BMSCs (lower panel). $n = 3$, *, $p < .05$. **(C):** H&E and **(D)** IHC staining from bone specimens of an osteoporotic patient. Left panel, NFI-C; middle panel, CD68; right panel, negative control. Scale bars = 50 μ m. $n = 3$. **(E):** Expression of *NFI-C* mRNA was analyzed from gene expression dataset GSE35959 deposited in gene expression omnibus. $n = 5$, *, $p < .05$. **(F):** Effect of H₂O₂ on NFI-C expression in hBMSCs. Real-time PCR and Western blot analyses were used to determine the level of NFI-C expression in hBMSCs treated with or without H₂O₂ (200 μ M/ml) for 5 days. $n = 3$, *, $p < .05$. Data are presented as the mean \pm SD. Abbreviations: hBMSCs, human bone marrow stromal cells; NFI-C, nuclear factor I-C; WT, wild type.

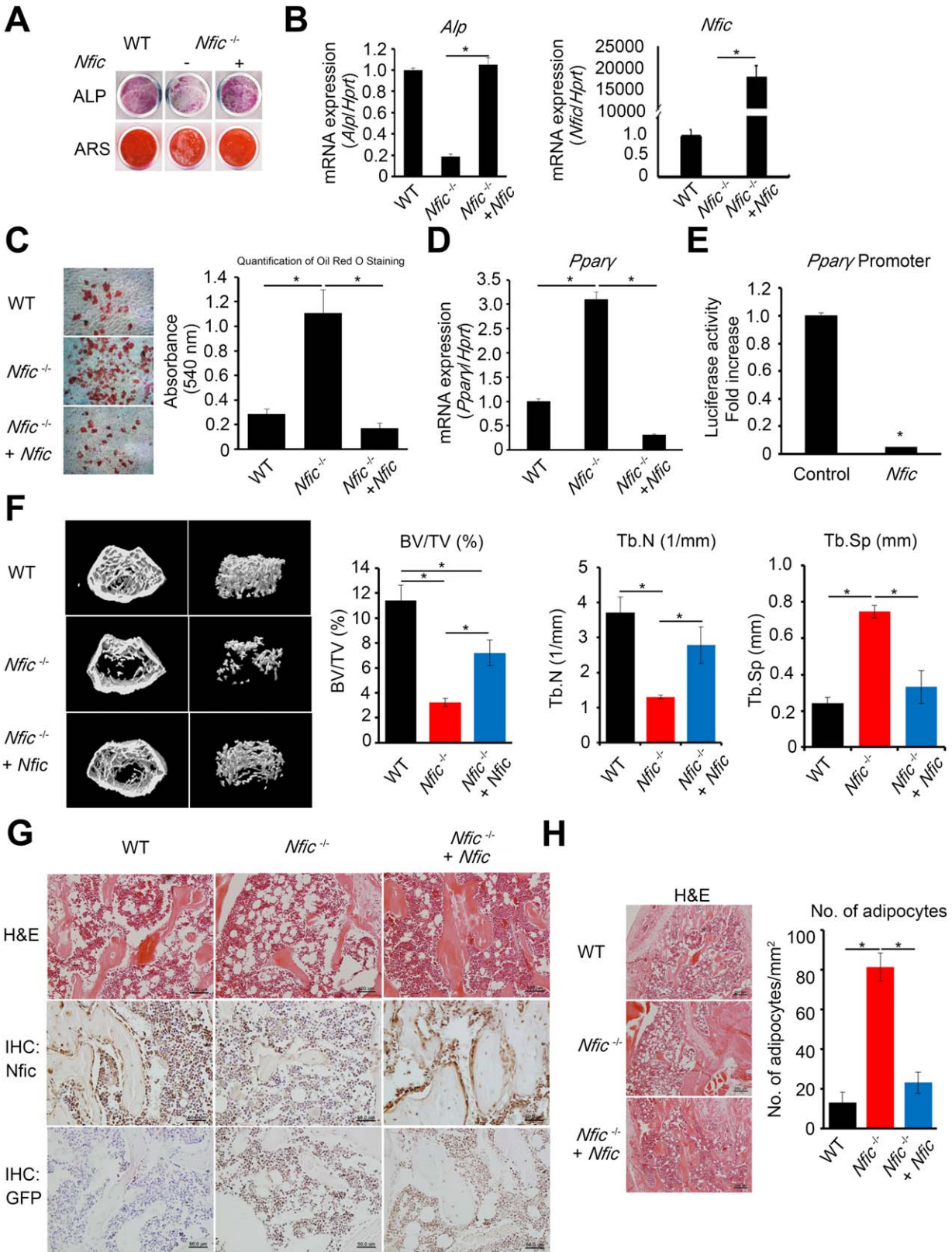


Figure 3. *Nfic* accelerates osteoblast differentiation and suppresses adipocyte differentiation. **(A)** *Nfic*^{-/-} bone marrow stromal cells (BMSCs) were transfected with the *Nfic* expression vector or control empty expression vector and then cultured in osteogenic induction media for 7 days (ALP staining) and 14 days (ARS). **(B)** *Alp* (left panel) and *Nfic* (right panel) expression were analyzed using real-time PCR. $n = 3$, $*$, $p < .05$. **(C)** Representative oil red O staining images (left panel) and quantification of oil red O staining (right panel). *Nfic*^{-/-} BMSCs were transfected with the *Nfic* expression vector or control empty expression vector and then cultured in adipogenic induction media for 7 days. **(D)** *Pparγ* expression was analyzed using real-time PCR. $n = 3$, $*$, $p < .05$. **(E)** *Pparγ* promoter activity was assessed in C2C12 cells transfected with pGL3-Luc-*Pparγ* and *Nfic* expression vectors or control empty expression vector for 48 hours. $n = 3$, $*$, $p < .05$. **(F)** Representative micro-CT images and micro-CT quantification of the distal femurs in WT and *Nfic*^{-/-} mice transplanted with *Nfic*-overexpressing BMSCs or mock-infected BMSCs at 10 weeks of age. $n = 3$, $*$, $p < .05$. **(G)** Histological analyses of distal femurs in *Nfic*^{-/-} mice transplanted with *Nfic*-overexpressing BMSCs. Immunohistochemistry (IHC) analysis of the femur transplanted with *Nfic*-overexpressed or mock-infected BMSCs using Nfic and GFP antibodies. Scale bars = 50 μ m. **(H)** H&E staining (left panel). Scale bars = 200 μ m. The number of adipocytes in *Nfic*^{-/-} mice transplanted with *Nfic*-overexpressing BMSCs compared to *Nfic*^{-/-} mice transplanted with mock-infected BMSCs at 10 weeks of age (right panel). $n = 3$, $*$, $p < .05$. Data are presented as the mean \pm SD. Abbreviations: ALP, alkaline phosphatase; ARS, alizarin red S staining; BV/TV, trabecular bone volume; GFP, green fluorescent protein; IHC, immunohistochemistry; Tb.N, trabecular bone number; Tb.Sp, trabecular separation; WT, wild type.

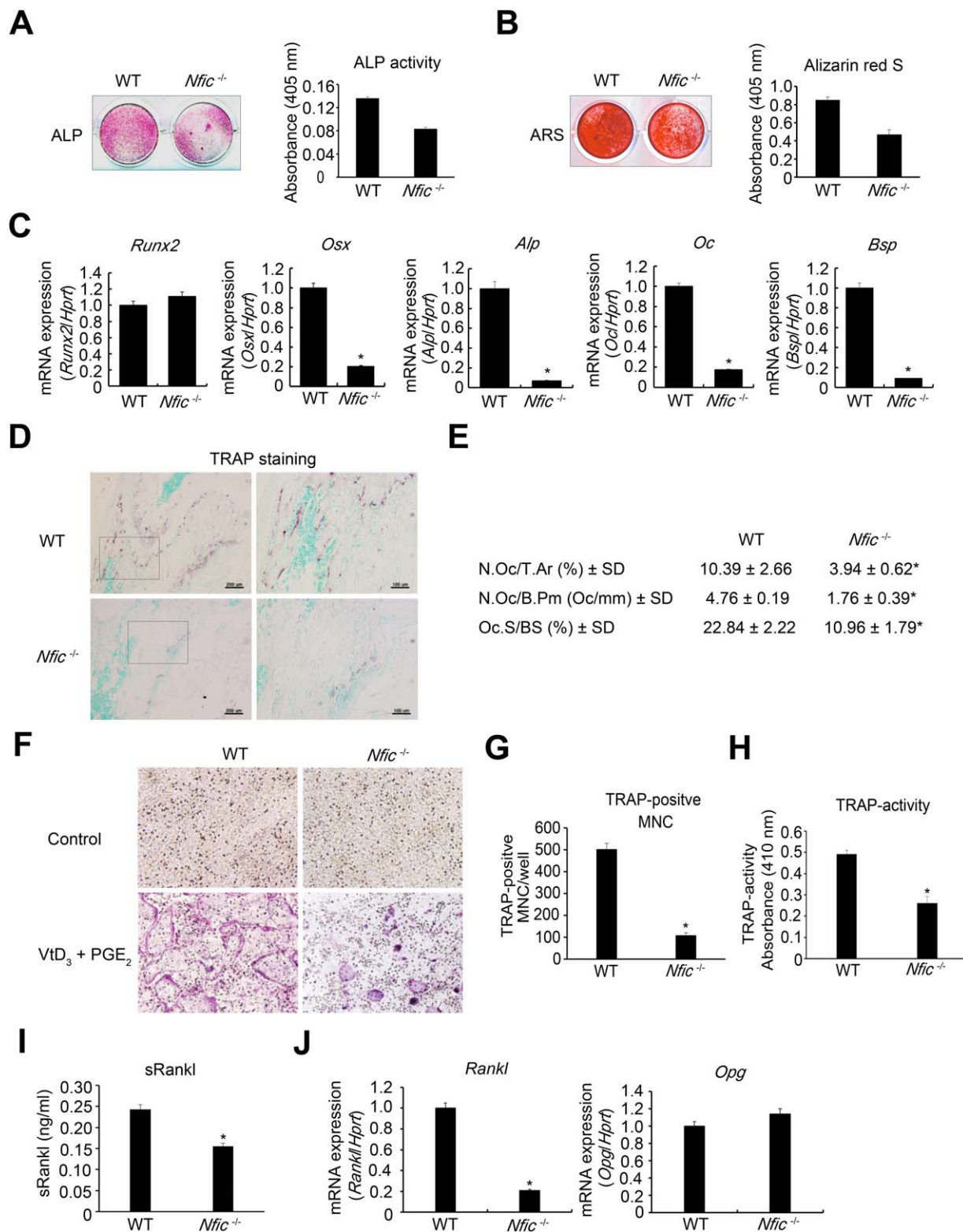


Figure 4. *Nfic* disruption impairs osteoblast differentiation and reduces osteoclast activity. **(A):** ALP staining and activity. **(B):** ARS and quantification of alizarin red S stained mineralized nodules. WT and *Nfic*^{-/-} bone marrow stromal cells (BMSCs) were cultured in osteogenic induction media for 7 days (ALP) and 14 days (ARS). $n = 3$, $p < .05$. **(C):** Expression of *Runx2*, *Osx*, *Alp*, *Oc*, and *Bsp* was analyzed using real-time PCR in WT and *Nfic*^{-/-} BMSCs after differentiation for 7 days. $n = 3$, $p < .05$. **(D):** TRAP staining of femurs from WT and *Nfic*^{-/-} mice aged 6 weeks. Right panels are higher magnifications of boxed left panels. Scale bars, right panels = 200 μ m; left panels = 100 μ m. **(E):** Histomorphometric analyses of the distal femoral metaphysis from WT and *Nfic*^{-/-} mice aged 6 weeks. $n = 5$, $p < .05$. **(F):** WT bone marrow-derived macrophages were cocultured with WT and *Nfic*^{-/-} primary osteoblasts for 6 days in the absence or presence of VitD₃ and PGE₂, fixed, and stained for TRAP. **(G):** TRAP-positive MNCs were counted in (D). $n = 3$, $p < .05$. **(H):** TRAP activity was quantified in cell lysates. $n = 3$, $p < .05$. **(I):** sRankl levels were measured in cell culture media using ELISA kits. $n = 3$, $p < .05$. **(J):** Expression of *Rankl* and *Opg* was analyzed in primary osteoblasts using real-time PCR. $n = 3$, $p < .05$. Data are presented as the mean \pm SD. Abbreviations: ALP, alkaline phosphatase; ARS, alizarin red S staining; MNCs, multinucleated cells; N.Oc/T.Ar, osteoclast number per tissue area; N.Oc/B.Pm, osteoclast number per bone parameter; Oc.S/BS, osteoclast surface per bone surface; PGE₂, prostaglandin E₂; TRAP, tartrate-resistant acid phosphatase; VitD₃, 1,25-dihydroxyvitamin D₃; WT, wild type.

mice, we evaluated TRAP activity in WT and *Nfic*^{-/-} mice at 6 weeks. The number of TRAP-positive osteoclasts was markedly decreased in *Nfic*^{-/-} mice compared to WT (Fig. 4D). In bone histomorphometric analyses, the osteoclast number per tissue area (N.Oc/T.Ar), osteoclast number per bone perimeter, and osteoclast surface per bone surface (Oc.S/BS) were significantly decreased in *Nfic*^{-/-} mice compared to WT at 6 weeks (Fig. 4E) as well as at P16 (Supporting Information Fig. S4A, S4B). Formation of multinucleated TRAP-positive osteoclasts in cultured BMMs was identical in both types of mice (Supporting Information Fig. S4C), suggesting that osteoclast lineage cells were not directly affected by *Nfic* disruption.

To determine whether impaired osteoblast differentiation in *Nfic*^{-/-} mice caused reduced osteoclast formation, we cocultured normal BMMs with WT or *Nfic*^{-/-} calvarial osteoblasts, and analyzed osteoclast generation by TRAP staining. The number of TRAP-positive multinucleated cells was significantly reduced when WT BMMs were cocultured with *Nfic*^{-/-} osteoblasts compared to WT osteoblasts (Fig. 4F, 4G). Osteoblasts from *Nfic*^{-/-} mice supported less osteoclastogenesis, and consequently decreased TRAP activity (Fig. 4H). Soluble RANKL (sRANKL) expression was also decreased in the *Nfic*^{-/-} osteoblast cocultured group (Fig. 4I). Using real-time PCR, we observed that osteoblasts from *Nfic*^{-/-} mice had normal expression of *osteoprotegerin* (*Opg*) but decreased *Rankl* expression (Fig. 4J). These results indicate that reduced osteoclast activity in *Nfic*^{-/-} mice may be due to the failure of normal osteoblast differentiation stemming from reduced RANKL-mediated signaling.

***Nfic* Mediates BMP2-Runx2-Induced *Osx* Expression**

Osx, a zinc finger-containing transcription factor, plays an important role in osteoblast differentiation [17]. To investigate the exact role of *Nfic* in osteoblast differentiation, we examined the interrelationship between *Nfic* and *Osx*. *Nfic*^{-/-} BMSCs exhibited reduced *Osx* mRNA expression compared to WT (Fig. 4C). The expression of *Osx* protein was dramatically reduced in *Nfic*^{-/-} osteoblasts compared to WT based on immunofluorescence of femoral trabecular bone, as well as by Western blot analyses (Fig. 5A, left panel), suggesting that *Nfic* is required for *Osx* expression. However, *Nfic*-disruption in mice did not alter the expression of Runx2 protein (Fig. 5A, right panel). *Osx* mRNA and protein levels were increased in *Nfic*-overexpressing cells (Fig. 5B). To assess the effects of *Nfic* on the transcriptional activity of the *Osx* promoter, we measured *Osx* promoter activity after overexpression of *Nfic* in MC3T3-E1 cells in the presence or absence of BMP-2. *Nfic*-overexpressing or BMP-2-treated cells increased *Osx* promoter activity. Moreover, *Nfic* overexpression strongly enhanced *Osx* promoter activity in the presence of BMP-2 (Fig. 5C) via a mechanism that includes direct binding to the *Osx* promoter region as determined by chromatin immunoprecipitation (ChIP) assays using the anti-*Nfic* antibody after BMP-2 treatment. We identified a putative *Nfic*-binding motif in a region between -359 and -117 of the *Osx* promoter in the presence of BMP-2 signaling (Fig. 5D). In addition, *Osx* expression was increased by BMP-2 treatment and/or *Nfic* overexpression in *Nfic*^{-/-} osteoblasts (Fig. 5E). These results suggest that *Nfic* directly regulates *Osx* expression through the BMP-2 signaling pathway during osteoblast differentiation. However, *Osx* expression was still detected in *Nfic*^{-/-} BMSCs. Interestingly,

Dlx5 and *Msx2* mRNA expression were significantly increased in *Nfic*^{-/-} mice compared to WT (Supporting Information Fig. S5A), suggesting that *Dlx5* and *Msx2* expression were increased in *Nfic*^{-/-} osteoblasts as a compensatory mechanism for *Osx* control. In addition, *Dlx5* or *Msx2* overexpression in *Nfic*^{-/-} osteoblasts significantly increased *Osx* expression compared to control osteoblasts (Supporting Information Fig. S5B).

To determine whether impaired bone formation could be rescued by *Osx* overexpression in *Nfic*^{-/-} mice, we overexpressed *Osx* in *Nfic*^{-/-} BMSCs via retroviral infection and transplanted them into the femur cavities of *Nfic*^{-/-} mice. Femur micro-CT images show that the trabecular bone volume reduction in *Nfic*^{-/-} mice was only partially rescued by *Osx* overexpression (Fig. 5F, left panel). In histomorphometric analyses, *Nfic*^{-/-} mice transplanted with *Osx*-overexpressing BMSCs exhibited significant increases in trabecular bone volume (BV/TV) and trabecular bone number (Tb.N), but significant decreases in Tb.SP (Fig. 5F, right panel). The transplanted BMSCs were analyzed by IHC using *Osx* and GFP antibodies 4 weeks after transplantation. *Osx*- and GFP-positive BMSCs were found in osteoblasts of the trabecular bone surface in *Nfic*^{-/-} mice transplanted with *Osx*-overexpressing BMSCs. However, in *Nfic*^{-/-} mice transplanted with mock-infected BMSCs, only GFP-positive BMSCs were found without *Osx* expression (Fig. 5G). In histological analyses, transplantation of *Osx*-overexpressing BMSCs increased trabecular bone mass, but marrow adiposity was unchanged (Fig. 5G). *Nfic*^{-/-} mice transplanted with *Osx*-overexpressing BMSCs was not altered in the number of adipocytes compared to *Nfic*^{-/-} mice (Fig. 5H). These results suggest that *Osx* promotes osteoblast differentiation but does not influence adipocyte differentiation in BMSCs.

***Runx2* Mediates BMP-2-Induced *Nfic* Expression**

Osteogenic transcription factors, including Runx2, *Dlx5*, *Msx2*, and *Osx*, are generally regulated by BMP-2 [5]. To investigate whether *Nfic* is regulated by BMP-2, we evaluated *Nfic* expression and promoter activity after BMP-2 stimulation in MC3T3-E1 cells using real-time PCR and Western blot. BMP-2 significantly increased *Nfic* promoter activity as well as *Nfic* mRNA and protein levels (Fig. 6A, 6C). We also examined whether Runx2, which is stimulated by BMP-2, regulates *Nfic* during osteogenesis. *Runx2* overexpression significantly increased *Nfic* promoter activity and *Nfic* mRNA and protein expression (Fig. 6B, 6C). *Runx2* knockdown decreased *Nfic* promoter activity and *Nfic* protein expression approximately 10-fold and inhibited the enhancing effect of BMP-2 on the *Nfic* promoter and expression (Fig. 6D). Next, to determine whether Runx2 directly binds to the *Nfic* promoter region, we performed ChIP assays using the Runx2 antibody after BMP-2 treatment. We identified a putative Runx2 consensus sequence in a region between -423 and -246 of the *Nfic* promoter. Runx2 directly interacted with the *Nfic* promoter in the presence of BMP-2 (Fig. 6E). In addition, we also examined *Nfic* expression in *Runx2*^{-/-} mice. In immunofluorescence studies, *Nfic* protein expression was observed but was dramatically reduced in *Runx2*^{-/-} developing bone and cartilage (Fig. 6F, upper panel). In real-time PCR and Western blot experiments, *Nfic* mRNA and protein expression levels were significantly decreased in *Runx2*^{-/-} mice compared to WT

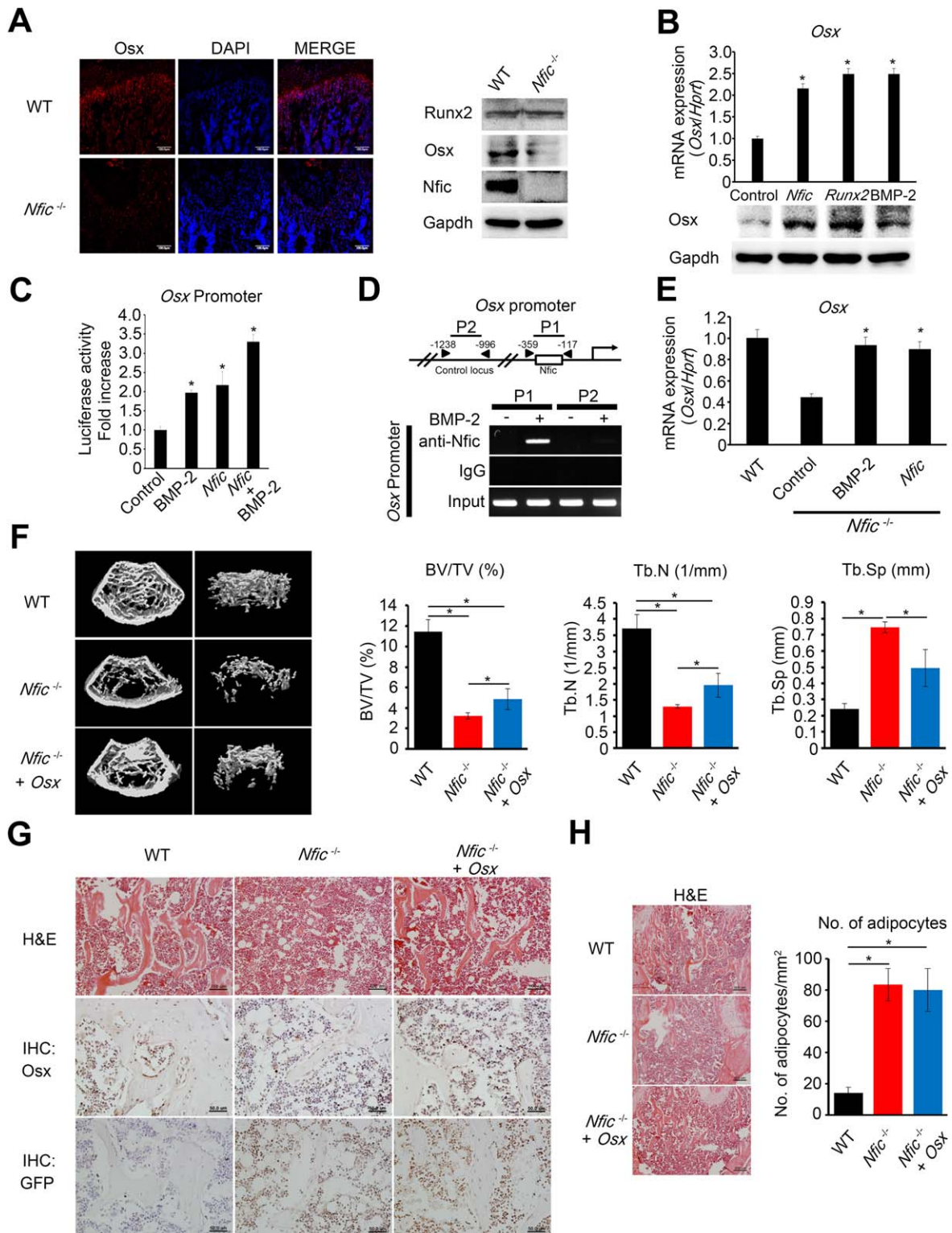


Figure 5. *Nfic* mediates BMP-2-*Runx2*-induced *Osx* expression. **(A)**: Immunofluorescence staining of *Osx* (red) in trabecular bone of distal femoral metaphysis from WT and *Nfic*^{-/-} mice aged 6 weeks. Scale bar = 100 μm. Western blotting analyses of *Runx2*, *Osx*, and *Nfic* in WT and *Nfic*^{-/-} bone marrow stromal cells (BMSCs). **(B)**: Real-time PCR and Western blot analyses to evaluate *Osx* expression in MC3T3-E1 cells transfected with *Nfic* and *Runx2* expression vectors or control empty expression vector and treated with BMP-2 (300 ng/ml) for 48 hours. *n* = 3, *, *p* < .05. **(C)**: *Osx* promoter activity assessed in MC3T3-E1 cells transfected with pGL3-Luc-*Osx* (-1,269 to +91) and *Nfic* expression vectors or control empty expression vector, and treated with BMP-2 (300 ng/ml) for 48 hours. *n* = 3, *, *p* < .05. **(D)**: Scheme of putative *Nfic*-binding motif in the *Osx* promoter. The primer pairs used for the ChIP assay are shown as arrowheads (upper panel). Detection of *Nfic* binding to the *Osx* promoter using ChIP analyses in MC3T3-E1 cells treated with BMP-2 (300 ng/ml) for 48 hours. The putative *Nfic*-binding motif was PCR-amplified with P1 primers, and a PCR was also performed with negative control locus primers P2 (lower panel). **(E)**: *Nfic*^{-/-} osteoblasts were treated with BMP-2 (300 ng/ml) and/or transfected with the *Nfic* expression vector. *Osx* expression was analyzed using real-time PCR. *n* = 3, *, *p* < .05. **(F)**: Representative micro-CT images and micro-CT quantification of the distal femurs in WT and *Nfic*^{-/-} mice transplanted with *Osx*-overexpressing BMSCs or mock-infected BMSCs at 10 weeks of age. *n* = 3, *, *p* < .05. **(G)**: Histological analyses of distal femurs in *Nfic*^{-/-} mice transplanted with *Osx*-overexpressing BMSCs. Immunohistochemistry (IHC) analysis of the femur transplanted with *Osx*-overexpressed or mock-infected BMSCs using *Osx* and GFP antibodies. Scale bars = 50 μm. **(H)**: H&E staining (left panel). Scale bars = 200 μm. The number of adipocytes in *Nfic*^{-/-} mice transplanted with *Osx*-overexpressing BMSCs compared to *Nfic*^{-/-} mice transplanted with mock-infected BMSCs at 10 weeks of age (right panel). *n* = 3, *, *p* < .05. Data are presented as the mean ± SD. Abbreviations: BMP-2, bone morphogenetic protein 2; BV/TV, trabecular bone volume; GFP, green fluorescent protein; IHC, immunohistochemistry; Tb.N, trabecular bone number; Tb.SP, trabecular separation; WT, wild type.

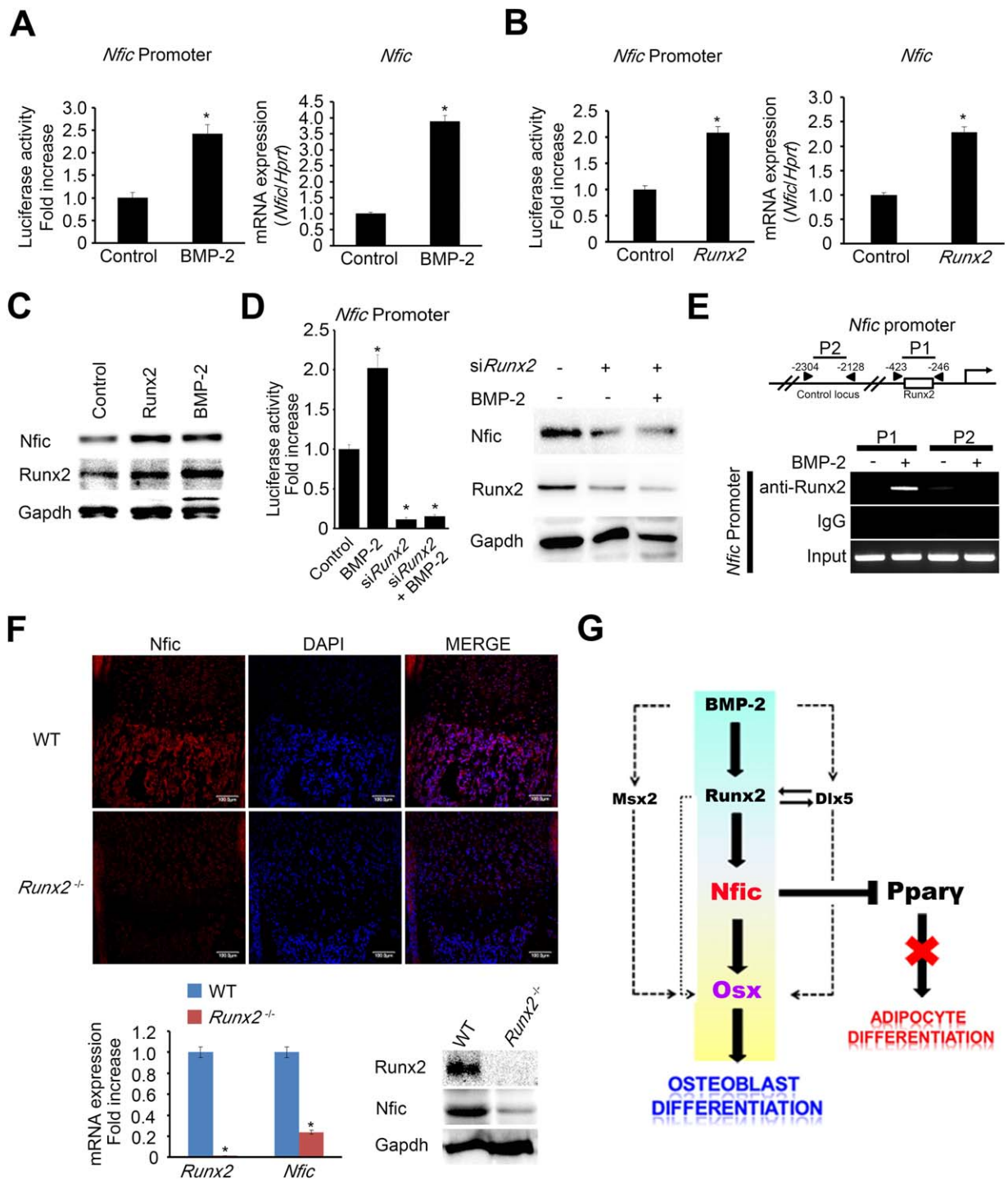


Figure 6. *Runx2* mediates BMP-2-induced *Nfic* expression. **(A, B)** *Nfic* promoter activity and mRNA expression were determined using promoter assays and real-time PCR in MC3T3-E1 cells transfected with pGL3-Luc-*Nfic* (−2,520 to +88) and *Runx2* expression vectors or control empty expression vector, and treated with BMP-2 (300 ng/ml) for 48 hours. *n* = 3, *, *p* < .05. **(C)** Western blot analyses to evaluate *Nfic* expression in MC3T3-E1 cells transfected with the *Runx2* expression vector or control empty expression vector and treated with BMP-2 (300 ng/ml) for 48 hours. **(D)** *Nfic* promoter activity was assessed in MC3T3-E1 cells transfected with pGL3-Luc-*Nfic* (−2,520 to +88) and *Runx2* siRNA or control siRNA in the presence or absence of BMP-2 (300 ng/ml) for 48 hours. *n* = 3, *, *p* < .05. *Nfic* and *Runx2* expression were analyzed using Western blot analyses in control and *Runx2*-inactivated MC3T3-E1 cells. **(E)** Scheme of putative *Runx2*-binding motif in the *Nfic* promoter. The primer pairs used for the ChIP assay were shown as arrowheads (upper panel). Detection of *Runx2* binding to the *Nfic* promoter using ChIP analyses in MC3T3-E1 cells treated with BMP-2 (300 ng/ml) for 48 hours. The putative *Runx2*-binding motif was PCR-amplified with P1 primers, and a PCR was also performed with negative control locus primers P2 (lower panel). **(F)** Immunofluorescence staining of *Nfic* (Red) in femurs from E18.5 WT and *Runx2*^{−/−} mice. Scale bar = 100 μm. Total RNA and protein isolated in calvarial bone from WT and *Runx2*^{−/−} mice. *Runx2* and *Nfic* expression were assessed using real-time PCR and Western blot analyses. *n* = 3, *, *p* < .05. Data are presented as the mean ± SD. **(G)** A model of role of *Nfic* during osteoblast and adipocyte differentiation. Abbreviations: BMP-2, bone morphogenetic protein 2; WT, wild type.

(Fig. 6F, lower panel). These results suggest that Runx2 acts upstream of *Nfic* and regulates *Nfic* expression through the BMP-2 signaling pathway.

DISCUSSION

Age-related osteoporosis is related to accumulation of bone marrow adiposity due to increased adipocyte differentiation rather than osteoblast differentiation in BMSCs of bone marrow [7]. In this study, we found that *Nfic* expression was decreased in an age-dependent manner. In addition, *Nfic*^{-/-} mice showed an age-related decrease in bone mass with a concomitant accumulation of marrow fat. *Nfic*^{-/-} mice show a similar bone phenotype to osteoporotic patients. PPAR γ is an important transcription factor controlling adipocyte differentiation [6]. In a previous study, it was reported that an NFI binding motif was found in the PPAR γ promoter region and that adipocyte differentiation increased due to upregulated PPAR γ expression mediated by NFI-A and NFI-B [18]. However, our findings show that *Nfic* inhibited adipocyte differentiation by suppressing PPAR γ expression in BMSCs, simultaneously increasing osteoblast differentiation. These results suggest that NFI-C controls the fate of BMSCs based on differentiation into osteoblasts and adipocytes.

The NFI gene family plays multiple essential roles in both prenatal and postnatal development. In *Nfia*^{-/-} and *Nfib*^{-/-} mice, the first morphological changes are observed at E14 to E15 [19]. *Nfia*^{-/-} mice showed prenatal lethality, which may be caused by defects in brain development [20], and *Nfib*^{-/-} mice also die at birth, likely due to lung maturation defects [19]. In contrast, *Nfix*^{-/-} mice exhibit a normal life span when their diet is supplemented with soft foods, suggesting they may have digestive tract defects [21]. Recently, it has been reported that Nfix is a novel regulator of hematopoietic stem and progenitor cell survival [22]. Nfix also modulates neuronal and glial differentiation during postnatal cerebellum development [23]. Similarly, *Nfic* acts as a regulator of postnatal growth and regeneration of adult progenitor cell proliferation and hair follicles [24]. *Nfic*^{-/-} mice have normal tooth crowns but short molar roots implying that *Nfic* has an essential role in stage-specific regulation of postnatal tooth development as molar root formation in mice starts around postnatal day 8 (~P8) [11, 25]. In this study, *Nfic*^{-/-} mice showed normal prenatal bone and tooth development but exhibited defects in postnatal bone growth. These findings indicate that NFI-C is an essential transcription factor that primarily regulates postnatal development in bone and tooth.

BMP-2 is a potent growth factor that promotes osteoblast differentiation and induces bone formation [26, 27]. BMP-2 cellular signaling regulates several osteogenic target transcription factors, including Runx2, Dlx5, Msx2, and Osx [26]. In this study, we demonstrated that the BMP-2 signaling pathway regulates *Nfic* expression. When BMP signaling is inhibited during bone and tooth development, noggin-overexpressing mice showed defects in the tooth root, impaired osteoblast differentiation, and reduced bone formation [28, 29] similar to the bone and tooth abnormalities shown in *Nfic*^{-/-} mice. Our study also demonstrated that Runx2-inactivated osteoblasts showed decreased *Nfic* expression and that BMP-2 induction in Runx2-inactivated osteoblasts could not reverse

this decrease in *Nfic*. Moreover, *Nfic* expression was dramatically decreased in *Runx2*^{-/-} mice, whereas *Nfic*^{-/-} osteogenic cells showed normal Runx2 expression. Overall, our results indicate that *Nfic* appears to function downstream of Runx2, and that BMP-2-induced *Nfic* expression is mediated by Runx2.

BMP-2 signaling regulates Osx expression, as well as Runx2, Dlx5, and Msx2 [30, 31]. It has been reported that Osx expression is regulated by BMP-2 signaling via both Runx2-dependent and -independent mechanisms. However, the mechanism by which BMP-2 regulates Osx expression remains unclear in some aspects. It is well known that Runx2 directly binds to Osx promoter region and regulates Osx promoter activity [32]. Accordingly, Runx2 overexpression significantly increased Osx expression in *Nfic*^{-/-} osteoblasts (data not shown). These findings suggest that Runx2 directly acts on Osx promoter. However, we for the first time suggest that Runx2-dependent Osx regulation in BMP-2 signaling is mediated in part by *Nfic*, which is a downstream target of Runx2. *Nfic* plays a role as an intermediary transducer between Runx2 and Osx in the BMP-2 signaling pathway during osteoblast differentiation. Dlx5 and Msx2 also regulate Osx expression through Runx2-independent pathways in BMP-2 signaling [30, 31]. In this study, our results suggest that Osx expression is regulated by BMP-2 signaling during osteoblast differentiation through three distinct mechanisms: the Runx2 pathway, the Runx2-*Nfic* pathway, and the Dlx5 and/or Msx2 pathway (Fig. 6G). Further investigation is required to determine the functional relationship among these three pathways in Osx regulation during osteoblast differentiation and bone formation.

Osx is an essential transcription factor for osteoblasts in embryonic skeletal development as well as during postnatal bone formation [17, 33]. In this study, *Nfic* disruption significantly decreased Osx expression and osteogenic cell number in *Nfic*^{-/-} mice during postnatal osteogenesis. In rescue experiments, transplantation of *Nfic*-overexpressing BMSCs dramatically increased bone mass compared to transplantation of Osx-overexpressing BMSCs in *Nfic*^{-/-} mice. Interestingly, *Nfic*^{-/-} mice transplanted with *Nfic*-overexpressing BMSCs decreased adipocyte differentiation and bone marrow adiposity, whereas those transplanted with Osx-overexpressing BMSCs were not altered. In accordance with our results, Osx enhanced osteoblast differentiation but did not influence adipocyte differentiation in BMSCs [34]. These data suggest that impaired bone formation in *Nfic*^{-/-} mice is caused by reduced Osx expression and osteogenic cell number as well as by increased adipocyte differentiation.

SUMMARY

In summary, our findings indicate that *Nfic* disruption alters the differentiation fate of BMSCs by inhibiting osteoblast differentiation and promoting adipocyte differentiation, thereby leading to age-related osteoporosis. Interestingly, transplantation of *Nfic*-overexpressing BMSCs rescued an osteoporosis-like phenotype in *Nfic*^{-/-} mice. Taken together, our data suggest that NFI-C is a new candidate gene that causes osteoporosis. Therefore, regulation of NFI-C expression in BMSCs

could be a novel therapeutic approach for treating osteoporosis.

ACKNOWLEDGMENTS

This work was supported by a National Research Foundation of Korea Grant (NRF-2013R1A2A2A01010911 and NRF-2013R1A2A1A01007642) and No. 2013070465 through the Oromaxillofacial Dysfunction Research Center for the Elderly at Seoul National University. We thank Toshihisa Komori (Department of Cell Biology, Nagasaki University Graduate School of Biomedical Sciences, Nagasaki, Japan) for providing *Runx2*^{-/-} mice.

REFERENCES

- 1 Prockop DJ. Marrow stromal cells as stem cells for nonhematopoietic tissues. *Science* 1997;276:71–74.
- 2 Tuli R, Tuli S, Nandi S et al. Characterization of multipotential mesenchymal progenitor cells derived from human trabecular bone. *Stem Cells* 2003;21:681–693.
- 3 Kobayashi T, Kronenberg H. Minireview: Transcriptional regulation in development of bone. *Endocrinology* 2005;146:1012–1017.
- 4 Marie PJ. Transcription factors controlling osteoblastogenesis. *Arch Biochem Biophys* 2008;473:98–105.
- 5 Nishimura R, Hata K, Matsubara T et al. Regulation of bone and cartilage development by network between BMP signalling and transcription factors. *J Biochem* 2012;151:247–254.
- 6 Takada I, Kouzmenko AP, Kato S. Wnt and PPARγ signaling in osteoblastogenesis and adipogenesis. *Nat Rev Rheumatol* 2009;5:442–447.
- 7 Kim M, Kim C, Choi YS et al. Age-related alterations in mesenchymal stem cells related to shift in differentiation from osteogenic to adipogenic potential: Implication to age-associated bone diseases and defects. *Mech Ageing Dev* 2012;133:215–225.
- 8 Chaudhry AZ, Lyons GE, Gronostajski RM. Expression patterns of the four nuclear factor I genes during mouse embryogenesis indicate a potential role in development. *Dev Dyn* 1997;208:313–325.
- 9 Gronostajski RM. Roles of the NFI/CTF gene family in transcription and development. *Gene* 2000;249:31–45.
- 10 Perez-Casellas LA, Wang X, Howard KD et al. Nuclear factor I transcription factors regulate IGF binding protein 5 gene transcription in human osteoblasts. *Biochim Biophys Acta* 2009;1789:78–87.
- 11 Steele-Perkins G, Butz KG, Lyons GE et al. Essential role for NFI-C/CTF transcription-replication factor in tooth root development. *Mol Cell Biol* 2003;23:1075–1084.
- 12 Wauquier F, Leotoing L, Coxam V et al. Oxidative stress in bone remodelling and disease. *Trends Mol Med* 2009;15:468–477.

AUTHOR CONTRIBUTIONS

D.-S.L.: designed, planned and coordinated the experiments, analyzed the data, and wrote the manuscript; J.-C.P.: coordinated and supervised the project and wrote the manuscript; H.-W.C., H.-J.K., Z.H.L., and H.-H.K.: performed the experiments; H.-M.R. and E.-S.C.: provided study design; R.M.G.: provided animals; Y.-I.Y.: provided and assessed clinical samples.

DISCLOSURE OF POTENTIAL CONFLICTS OF INTEREST

The authors indicate no potential conflicts of interest.

- 13 Morel Y, Barouki R. The repression of nuclear factor I/CCAAT transcription factor (NFI/CTF) transactivating domain by oxidative stress is mediated by a critical cysteine (Cys-427). *Biochem J* 2000;348 Pt 1:235–240.
- 14 Lee DS, Park JT, Kim HM et al. Nuclear factor I-C is essential for odontogenic cell proliferation and odontoblast differentiation during tooth root development. *J Biol Chem* 2009;284:17293–17303.
- 15 Oh HJ, Lee HK, Park SJ et al. Zinc balance is critical for NFI-C mediated regulation of odontoblast differentiation. *J Cell Biochem* 2012;113:877–887.
- 16 Benisch P, Schilling T, Klein-Hitpass L et al. The transcriptional profile of mesenchymal stem cell populations in primary osteoporosis is distinct and shows overexpression of osteogenic inhibitors. *PLoS One* 2012;7:e45142.
- 17 Nakashima K, Zhou X, Kunkel G et al. The novel zinc finger-containing transcription factor osterix is required for osteoblast differentiation and bone formation. *Cell* 2002;108:17–29.
- 18 Waki H, Nakamura M, Yamauchi T et al. Global mapping of cell type-specific open chromatin by FAIRE-seq reveals the regulatory role of the NFI family in adipocyte differentiation. *PLoS Genet* 2011;7:e1002311.
- 19 Steele-Perkins G, Plachez C, Butz KG et al. The transcription factor gene Nfib is essential for both lung maturation and brain development. *Mol Cell Biol* 2005;25:685–698.
- 20 das Neves L, Duchala CS, Tolentino-Silva F et al. Disruption of the murine nuclear factor I-A gene (*Nfia*) results in perinatal lethality, hydrocephalus, and agenesis of the corpus callosum. *Proc Natl Acad Sci USA* 1999;96:11946–11951.
- 21 Campbell CE, Piper M, Plachez C et al. The transcription factor Nfix is essential for normal brain development. *BMC Dev Biol* 2008;8:52.
- 22 Holmfeldt P, Pardieck J, Saulsberry AC et al. Nfix is a novel regulator of murine hematopoietic stem and progenitor cell survival. *Blood* 2013;122:2987–2996.
- 23 Piper M, Harris L, Barry G et al. Nuclear factor one X regulates the development of

- multiple cellular populations in the postnatal cerebellum. *J Comp Neurol* 2011;519:3532–3548.
- 24 Plasari G, Edelmann S, Hogger F et al. Nuclear factor I-C regulates TGF-β-dependent hair follicle cycling. *J Biol Chem* 2010;285:34115–34125.
- 25 Park JC, Herr Y, Kim HJ et al. Nfic gene disruption inhibits differentiation of odontoblasts responsible for root formation and results in formation of short and abnormal roots in mice. *J Periodontol* 2007;78:1795–1802.
- 26 Chen G, Deng C, Li YP. TGF-β and BMP signaling in osteoblast differentiation and bone formation. *Int J Biol Sci* 2012;8:272–288.
- 27 Wan M, Cao X. BMP signaling in skeletal development. *Biochem Biophys Res Commun* 2005;328:651–657.
- 28 Plikus MV, Zeichner-David M, Mayer JA et al. Morphoregulation of teeth: Modulating the number, size, shape and differentiation by tuning Bmp activity. *Evol Dev* 2005;7:440–457.
- 29 Wu XB, Li Y, Schneider A et al. Impaired osteoblastic differentiation, reduced bone formation, and severe osteoporosis in noggin-overexpressing mice. *J Clin Invest* 2003;112:924–934.
- 30 Matsubara T, Kida K, Yamaguchi A et al. BMP2 regulates osterix through Msx2 and Runx2 during osteoblast differentiation. *J Biol Chem* 2008;283:29119–29125.
- 31 Lee MH, Kwon TG, Park HS et al. BMP-2-induced osterix expression is mediated by Dlx5 but is independent of Runx2. *Biochem Biophys Res Commun* 2003;309:689–694.
- 32 Nishio Y, Dong Y, Paris M et al. Runx2-mediated regulation of the zinc finger Osterix/Sp7 gene. *Gene* 2006;372:62–70.
- 33 Zhou X, Zhang Z, Feng JQ et al. Multiple functions of osterix are required for bone growth and homeostasis in postnatal mice. *Proc Natl Acad Sci USA* 2010;107:12919–12924.
- 34 Tu Q, Valverde P, Chen J. Osterix enhances proliferation and osteogenic potential of bone marrow stromal cells. *Biochem Biophys Res Commun* 2006;341:1257–1265.



See www.StemCells.com for supporting information available online.